Computational and Theoretical Chemistry 993 (2012) 45–52

Contents lists available at SciVerse ScienceDirect

Computational and Theoretical Chemistry

journal homepage: www.elsevier.com/locate/comptc

The adsorption and reactions of $SiCl_x$ (x = 0–4) on hydroxylated TiO_2 anatase (1 0 1) surface: A computational study on the functionalization of titania with $Cl_2Si(O)O$ adsorbate

Wen-Fei Huang [a], Hsin-Tsung Chen [b,*], M.C. Lin [a,*]

[a] Center of Interdisciplinary Molecular Science, National Chiao Tung University, Hsinchu 300, Taiwan
[b] Department of Chemistry, Chung Yuan Christian University, Chungli 32023, Taiwan

ARTICLE INFO

Article history:
Received 21 April 2012
Received in revised form 22 May 2012
Accepted 22 May 2012
Available online 5 June 2012

Keywords:
$SiCl_x$ adsorption
Hydroxylated TiO_2
Density functional theory

ABSTRACT

The adsorption and reactions of the $SiCl_x$ (x = 0–4) on the hydroxylated TiO_2 anatase (1 0 1) surface have been investigated by using periodic density functional theory calculations in conjunction with the projected augmented wave (PAW) approach. The adsorption and reactions tend to occur more readily on the 'O_w' site derived from water than the 'O_s' site from TiO_2 as revealed by the potential energy profiles and adsorption energies. The stepwise reactions of $SiCl_x$ can be achieved by dehydrochlorination taking place by three paths: O_w-path, cross-path, and O_s-path. The O_w-path is the lowest energy path, in which **$Cl_3Si–O_w$(a)** and **$Cl_2Si–(O_w)O_w$(a)** are the main products formed by spontaneous reactions. The ready formation and the high stability of **$Cl_2Si–(O_w)O_w$(a)** suggest that it can be employed as a molecular linker for Si and other semiconductor quantum dot growth on titania through its high reactivity towards SiH_x radicals and metal alkyls, respectively.

1. Introduction

Titanium dioxide (TiO_2) has been shown to be a very versatile material as demonstrated in numerous theoretical and experimental studies because of its promising applications to fabrication of photocatalysts and photoelectrochemical devices [1,2]. The photophysics of TiO_2 sensitized by a variety of dyes [3–5], polymers [6,7], and semiconductors [8–10] have been widely studied in particular for solar energy conversions. One of the well-known semiconductor quantum dots for solar cell applications is silicon, which has been studied extensively [11–20]. In 2004, the growth of Si on TiO_2 rutile (1 1 0) surface was reported by Abad et al. [21].

To improve the heterogeneous interface and achieve higher photovoltaic efficiencies, inorganic linkers have been employed for semiconductor quantum dots growth on TiO_2 [22–27]. Inorganic linkers for pure TiO_2 anatase (1 0 1) and rutile (1 1 0) surfaces, SiH_x, have been studied theoretically by Huang et al. [28]. However, the TiO_2 surface is known to be readily covered with hydroxyl groups in the water-rich environment [29–33]. SiH_x, particularly SiH_4, was found to interact weakly with the hydroxylated TiO_2 surface and thus may not be a good linker between silicon and hydroxylated TiO_2 surface. Based on the known propensity of $SiCl_4$ reactions with HO-containing molecules and their common use as Si sources in the silica-coating process [34,35], $SiCl_x$ (x = 1–4) is expected to be a potential linker for the hydroxylated TiO_2 surface.

In this work, we study the adsorption of $SiCl_x$ with the hydroxylated TiO_2 anatase (1 0 1) surface as well as their decomposition reactions by dehydrochlorination employing the density functional theory (DFT). The potential energy profiles of the reactions are calculated by nudged elastic band (NEB) method. The results of this study should be useful for understanding the mechanism for $SiCl_x$ adsorption and decomposition on the TiO_2 surface for fabrication of optoelectronic devices and solar cells.

2. Computational methods and models

All calculations were performed by the spin-polarized DFT with the projected augmented wave method (PAW) [36] as implemented in the Vienna ab initio simulation package (VASP) [37,38]. The ionic cores were described by the generalized gradient approximation (GGA) with the PW91 [39] formulation which had been shown to work well for gas-surface reactions [22,27,40,41]. The electronic orbitals were represented by the plane-wave expansion including all the plane waves with their kinetic energies smaller than the chosen cut-off energy, $\hbar k^2/2\ m < E_{cut}$ (500 eV), which ensures the convergence. The nudged elastic band (NEB) method [42] was applied to locate the transition states (TSs), up to eight images for each calculated TS. All the transition structures were verified by the frequency calculations.

* Corresponding authors.
E-mail addresses: htchen@cycu.edu.tw (H.-T. Chen), chemmcl@emory.edu (M.C. Lin).

2210-271X/$ - see front matter © 2012 Elsevier B.V. All rights reserved.
http://dx.doi.org/10.1016/j.comptc.2012.05.035

The TiO_2 NP film is a polycrystalline material with different phases dependent on annealing temperature [43–45], particle size [46–48], and shape [49]. The three different phases of TiO_2 are rutile, anatase, and brookite. For solar cell applications, Park et al. showed that electron transport is slower in rutile films by intensity-modulated photocurrent and scanning electron microscopy [50]. Anatase is the preferred phase of TiO_2 for catalysis, photocatalysis, and solar cell applications [1,2,51,52], and (101) is the most stable surface of the anatase surface [53]. Hence, we attempt to characterize $SiCl_x$ reactions on the TiO_2 anatase (101) surface in this study.

The bulk TiO_2 was optimized first with $(4 \times 4 \times 4)$ Monkhorst-Pack k-points. Based on the optimized bulk TiO_2 geometry, the surface super cell consisting of 24 [TiO_2] units (three Ti layers, see Supporting Information) was modeled as periodically repeated slabs, separated by a vacuum space greater than 13 Å, which guaranties no interactions between the slabs. The lowest layers of each slab were fixed to preserve the calculated bulk parameters, while the remaining layers were fully relaxed to simulate the surface behavior during the calculations. The $(4 \times 6 \times 1)$ Monkhorst-Pack k-points were used for the TiO_2 surface calculation. Gas-phase molecules were simulated in a 20 Å cubic box, which is large enough to ignore interactions between each periodic gas molecules.

3. Results and discussion

To verify the reliability of the computational results, we first compared the calculated bulk lattice constants with experimental values. The predicted lattice constants of TiO_2 anatase are $a = 3.824$ Å and $c = 9.678$ Å, which are in good agreement with the experimental values, [54,55] $a = 3.872$–3.875 Å and $c = 9.502$–9.514 Å. The predicted fractional coordinate is $u = 0.208$, which also agrees well with the experimental value, $u = 0.208$ [56]. In addition, the predicted adsorption energy of H_2O on TiO_2 anatase (101) surface is also in good agreement with experimental results, which will be discussed below. The good prediction of bulk geometry and adsorption energy of H_2O on TiO_2 anatase (101) surface supports the validity of the surface model. The geometries of gas phase molecules, $SiCl_x$(g) ($x = 1$–4), are also examined, and the comparison of the experimental and calculated results is made in Table S1 of Supporting Information. Our predicted results are in very good agreement with the experimental and other calculated data.

3.1. Hydroxylated TiO_2 anatase (101) surface

The generally accepted scheme for the formation of hydroxylated TiO_2 surface(29–33) is shown in Fig. 1a. There are four different adsorption sites on the clean TiO_2 surfaces: Ti_{5c} (fivefold coordinated titanium), Ti_{6c} (sixfold coordinated titanium), O_{2c} (twofold coordinated oxygen or bridged oxygen), and O_{3c} (threefold coordinated oxygen). The two unsaturated sites, Ti_{5c} and O_{2c}, are more reactive [57,58]. In the hydroxylation reaction, H_2O molecule firstly adsorbs at the Ti_{5c} site, forming **H_2O–Ti_{5c}(a)**, and then dissociates to HO and H as described below. The H atom binds to the bridge oxygen (O_{2c}) and co-adsorbs with the HO radical at the Ti_{5c} site forming **HO–Ti_{5c},H–O_{2c}(a)**. All the calculated energies at 1 ML are also shown in Fig. 1a. The adsorption energy of **H_2O–Ti_{5c}(a)** at 1 ML is 17.3 kcal/mol, which is in good agreement with calculated (15.9–16.6 kcal/mol) [57,59,60] and experimental (16.6–17.1 kcal/mol)[61] results. The transition state lies 5.0 kcal/mol below the reactants, TiO_2(s) + H_2O(g); the overall reaction is exothermicity of 10.3 kcal/mol. Hence, the formation of the hydroxylated TiO_2 is a spontaneous reaction, as observed experimentally [29,32,62].

There are two types of hydroxyl groups on the TiO_2 surface. One derived from the H_2O molecule, and the other one is formed by H reaction with the O_{2c} of the TiO_{2c} surface. To distinguish the two types of oxygen sources, we name the O atoms from H_2O and TiO_2 as 'O_w' and 'O_s', respectively. The calculated geometry of the fully hydroxylated TiO_2 anatase (101) surface is shown in Fig. 1b. The bond length and bond angles of H–O_w and H–O_w–Ti_{5c} are 0.971 Å and 122.7°, respectively, while those for H–O_s and H–O_s–Ti_{5c} are 0.972 Å and 121.3°. A Bader atomic charge analysis [63] shows the two types of hydroxyl groups have similar charge distribution. The charges of two H atoms are 1.00 e, and those of 'O_w' and 'O_s' are 1.67 e and 1.60 e.

However, the reactivities of these two types of hydroxyl groups are different due to the surface morphology. The 'O_w' and 'O_s' atoms lie above the first Ti layer by 1.822 and 0.627 Å respectively. In other words, 'O_w' protrudes out of the surface more evidently than 'O_s' does. Thus gas molecule can more easily adsorb on the 'O_w' site than on the 'O_s' site as will be reflected by the differences

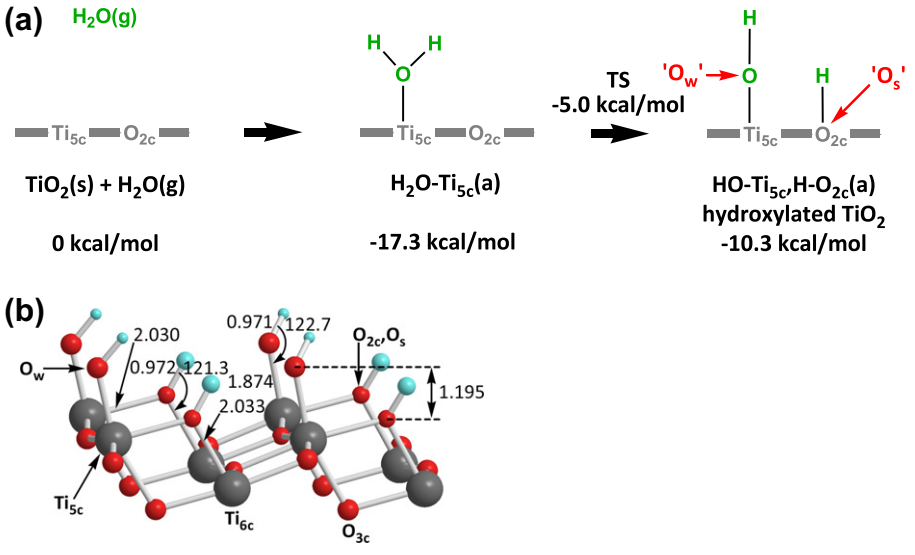

Fig. 1. (a) Scheme of the formation of hydroxylated TiO_2 surface. All the energies are referred to the energy of TiO_2(s) + H_2O(g). (b) The configuration of fully hydroxylated TiO_2 anatase (101) surface. TiO_2 model is only shown with one Ti layer. The bond length and angle are in Å and degree, respectively.

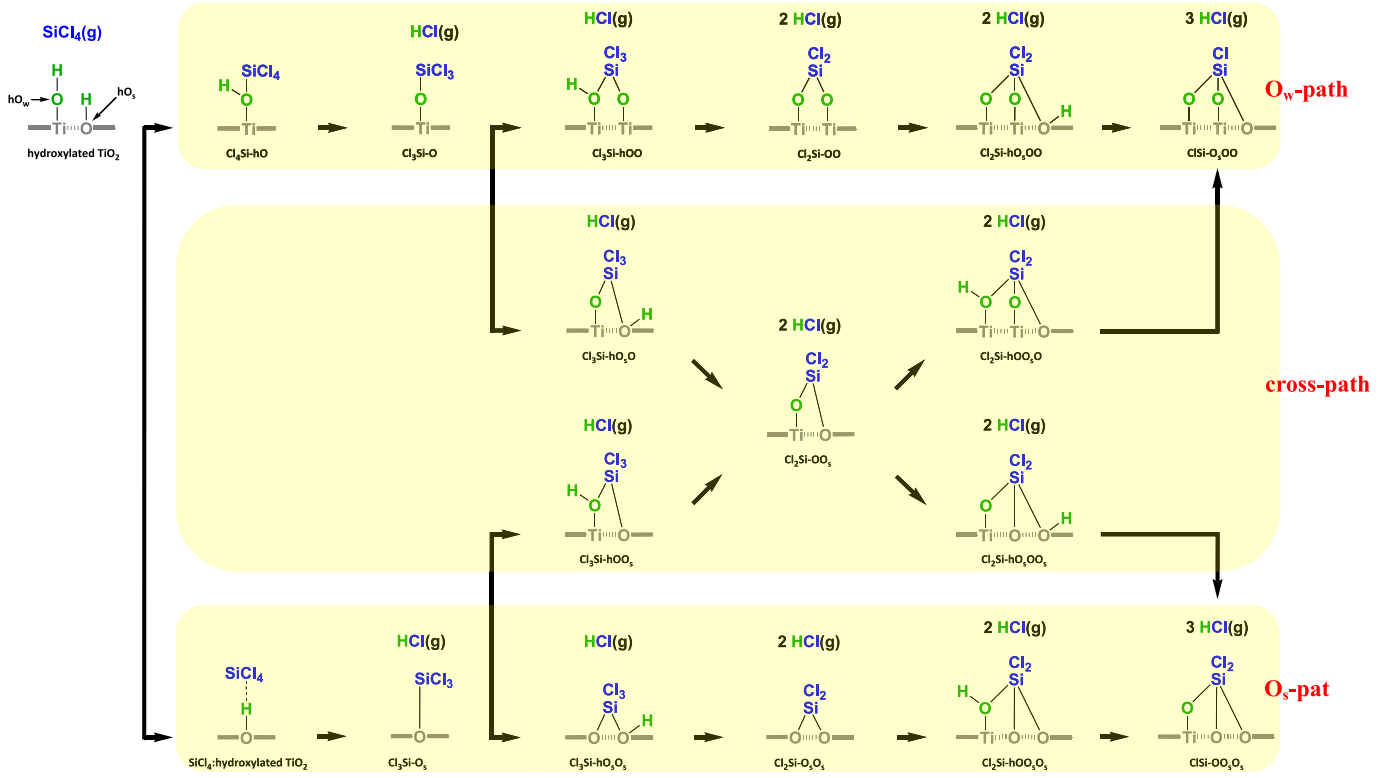

Fig. 2. Scheme of $SiCl_x$ decomposition on the hydroxylated TiO_2 anatase (1 0 1) surface. (For the surface sketch, only the adsorbed sites are shown. The reactions are all in mass balance.)

in adsorption energies and potential energy profiles discussed below.

3.2. Adsorption and reactions of $SiCl_x$ (x = 0–4) on the TiO_2 anatase (1 1 0) surface

To generalize the nomenclature, **Cl_xSi–(h)P_1…P_y(a)** (P_1…P_y = O_w or O_s) is named for $SiCl_x$ adsorbates formed by the Si head bonding with P_1, P_2…P_y sites, which can be one to three sites (y = 1–3). The prefixed 'h' denotes an H atom adsorbed concurrently on the P_1 site. For example, **Cl_xSi–hO_sO_w(a)** represents $SiCl_x$ doubly bonded with O_s and O_w atoms with a hydrogen atom simultaneously bonding with the O_s atom.

3.2.1. Dehydrochlorination reactions

Atomic layer growth of metal oxide can occur on a hydroxylated surface with MCl_4 (M = Si [64] or Ti [65]) by dehydrochlorination. A general reaction can be illustrated by $HO(a) + MCl_4(g) \rightarrow Cl_3MO(a) + HCl(g)$. HCl can be formed from the reaction of one of the Cl atoms of MCl_4 with one of the H atoms on the hydroxylated surface. Hence, $SiCl_x$ decomposition on the hydroxylated TiO_2 surface can be achieved by a similar dehydrochlorination reaction.

The possible mechanisms of $SiCl_x$ decomposition reactions are shown in Fig. 2. Three reaction pathways are considered. The reaction following the 'O_w' bonding site first (the order is O_w–O_w–O_s) is named O_w-path, and the one following the 'O_s' bonding site first (the order is O_s–O_s–O_w) is named O_s-path. The remaining reaction is named cross-path, which may have the order of O_w–O_s–O_w or O_s–O_w–O_s.

3.2.2. The lowest energy path

In our calculations, we find that the O_w-path is the lowest energy path, and the O_s-path is the highest energy path. The complete potential energy profiles are shown in Supporting Information of Fig. S2. As shown in the figure, the highest energy barriers of the O_w-path, cross-path and O_s-path are 9.7, 15.9, and 37.6 kcal/mol, respectively. As mentioned above, the gas molecule can attach to the protruding 'O_w' site more readily than to the 'O_s' site. In the following, we only discuss the O_w-path mechanism.

Fig. 3 shows the potential energy profile describing the O_w-path mechanism. The simplified geometries depicted in Fig. 3 are shown in Fig. 4. As illustrated in Fig. 3a, $SiCl_4$ physically associates with one of the O_w atoms on the fully hydroxylated TiO_2 anatase surface firstly with an association energy of 11.5 kcal/mol and the Si…O_w distance of 3.926 Å. Overcoming a small energy barrier of 7.2 kcal/mol (**TS1**, Fig. 4b), the $SiCl_4$ molecule can chemically bond with the surface with an Si–O_w bond of 1.753 Å, forming **Cl_4Si–hO_w(a)** (Fig. 4c) with an exothermicity of 7.7 kcal/mol. The surrounding H atoms can undergo hydrogen-bonding with the Cl atoms in **Cl_4Si–hO_w(a)**. Dehydrochlorination occurs when one of the Cl atoms is attracted by one of the nearest H atoms on the hydroxylated surface; the barrier for the process at **TS2** is 14.1 kcal/mol below the reactants (Fig. 4d), giving an H…Cl bonding complex **M1** (Fig. 4e) with an overall exothermicity of 21.8 kcal/mol. The distances of Cl…Si and Cl…H of **M1** are 3.671 and 1.874 Å, respectively. Crossing the small **TS3** (Fig. 4f) barrier of 4.6 kcal/mol, one HCl molecule is produced to form a hydrogen bonding complex **HCl:Cl_3Si–O_w(a)** (Fig. 4g) with an overall exothermicity of 24.0 kcal/mol. The physically adsorbed HCl(g) can be released endothermically with 3.6 kcal/mol, producing **Cl_3Si–O_w(a)** (Fig. 4h) on the surface which has a binding energy as high as 133 kcal/mol (see Table 1).

Starting from **Cl_3Si–O_w(a)**, the Si atom can doubly bond with another oxygen atom of 'O_w(H)' to form **Cl_3Si–hO_wO_w(a)** (Fig. 4j) by overcoming the **TS4** barrier of 14.8 kcal/mol; the complex lies 4.5 kcal/mol below the initial reactants. The bond lengths of Si–O_w and Si–O_w(H) are 1.643 and 1.896 Å, respectively. The longer bond length of Si–O_w(H) resulted from the additional bonding with the hydrogen atom. The over-bonding of the Si atom in

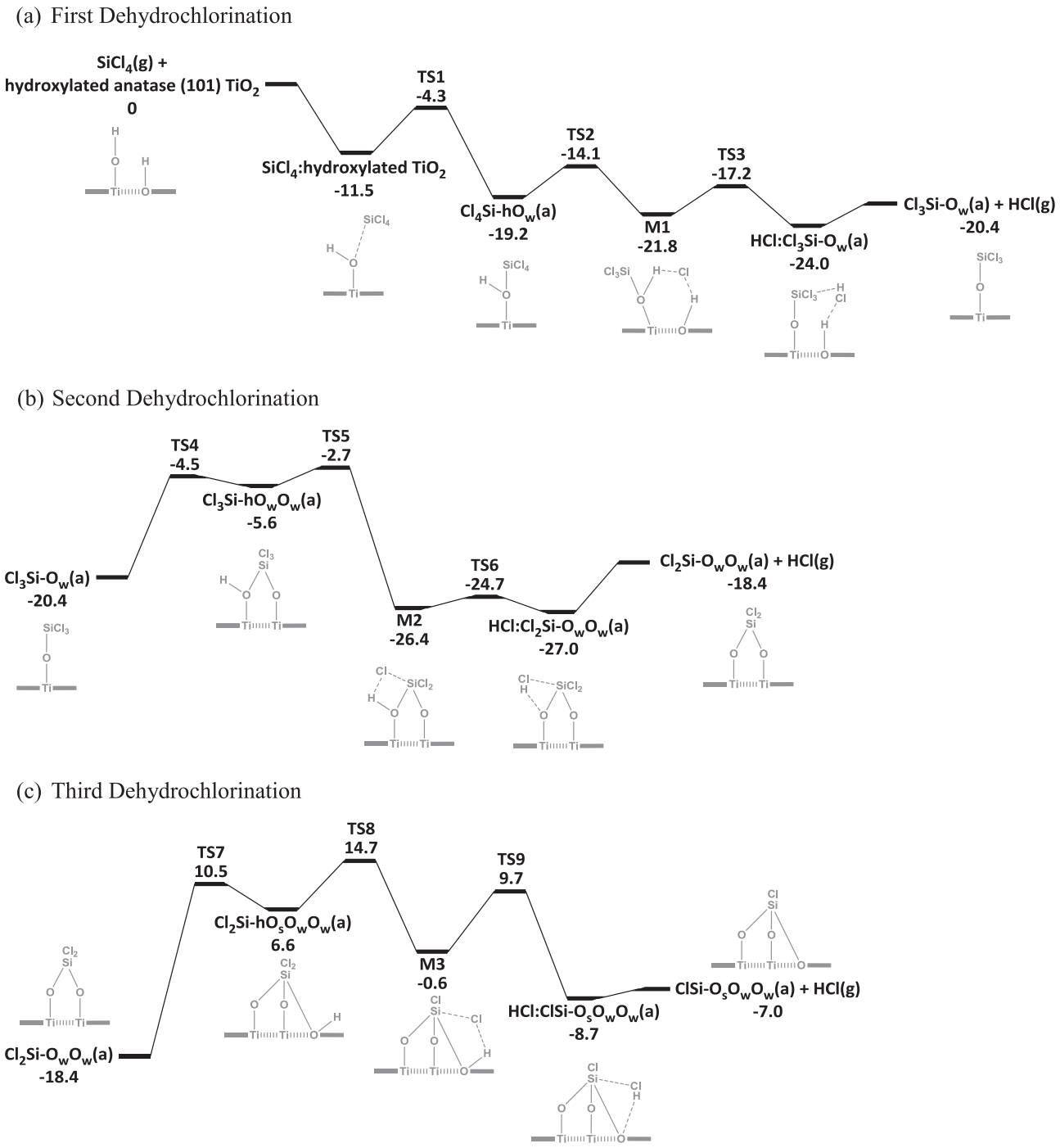

Fig. 3. Schematic potential energy profiles for the most possible reaction path of $SiCl_x$ decomposition on the hydroxylated TiO_2 anatase (1 0 1) surface. (For the surface sketch, only the adsorbed sites are shown. In figure (b) and (c), one and two HCl(g) are omitted for brevity, respectively; they are included in energy calculations and are mass-balanced.)

$Cl_3Si–hO_wO_w$(a) enhances the hydrogen bonding between one of Cl atoms with the H attached to the O_w atom bonding with Si by overcoming a small energy barrier of 2.9 kcal/mol (**TS5**, Fig. 4k) forming the intermediate **M2** (Fig. 4i) in which the Cl…H distance is 1.827 Å. The second dehydrochlorination can be achieved readily by overcoming a small barrier **TS6** (Fig. 4m) of 1.7 kcal/mol, giving **HCl:$Cl_2Si–O_wO_w$(a)** (Fig. 4n) with a small exothermicity of 0.6 kcal/mol. The desorption of the physically adsorbed HCl(a) requires 8.6 kcal/mol to give the highly stable, doubly bonded **$Cl_2Si–O_w$-O_w(a)** (Fig. 4o) on the surface. Similar to the reaction of $Cl_3Si–O_w(a) \rightarrow Cl_3Si–hO_wO_w(a)$, the Si atom of **$Cl_2Si–O_wO_w$(a)** can triply bond with one more closest oxygen site, 'O_s', forming **$Cl_2Si–hO_s$-O_wO_w(a)** (Fig. 4q) by overcoming a high energy barrier of 28.9 kcal/mol (**TS7**, Fig. 4p) with an endothermicity of 25.0 kcal/mol. The high energy barrier and the endothermicity for the formation of the triply bonded adsorbate make the doubly bonded **$Cl_2Si–O_wO_w$(a)** adsorbate the major terminal product. Due to the surface morphology, it is also impossible to attach to another 'O_w' site for **$Cl_2Si–O_wO_w$(a)** along the O_w-path. One of Cl atoms in **$Cl_2Si–hO_s$-O_wO_w(a)** can in principle undergo further dehydrochlorination through hydrogen bonding to form the third intermediate **M3** (Fig. 4s) with an exothermicity of 7.2 kcal/mol by overcoming the

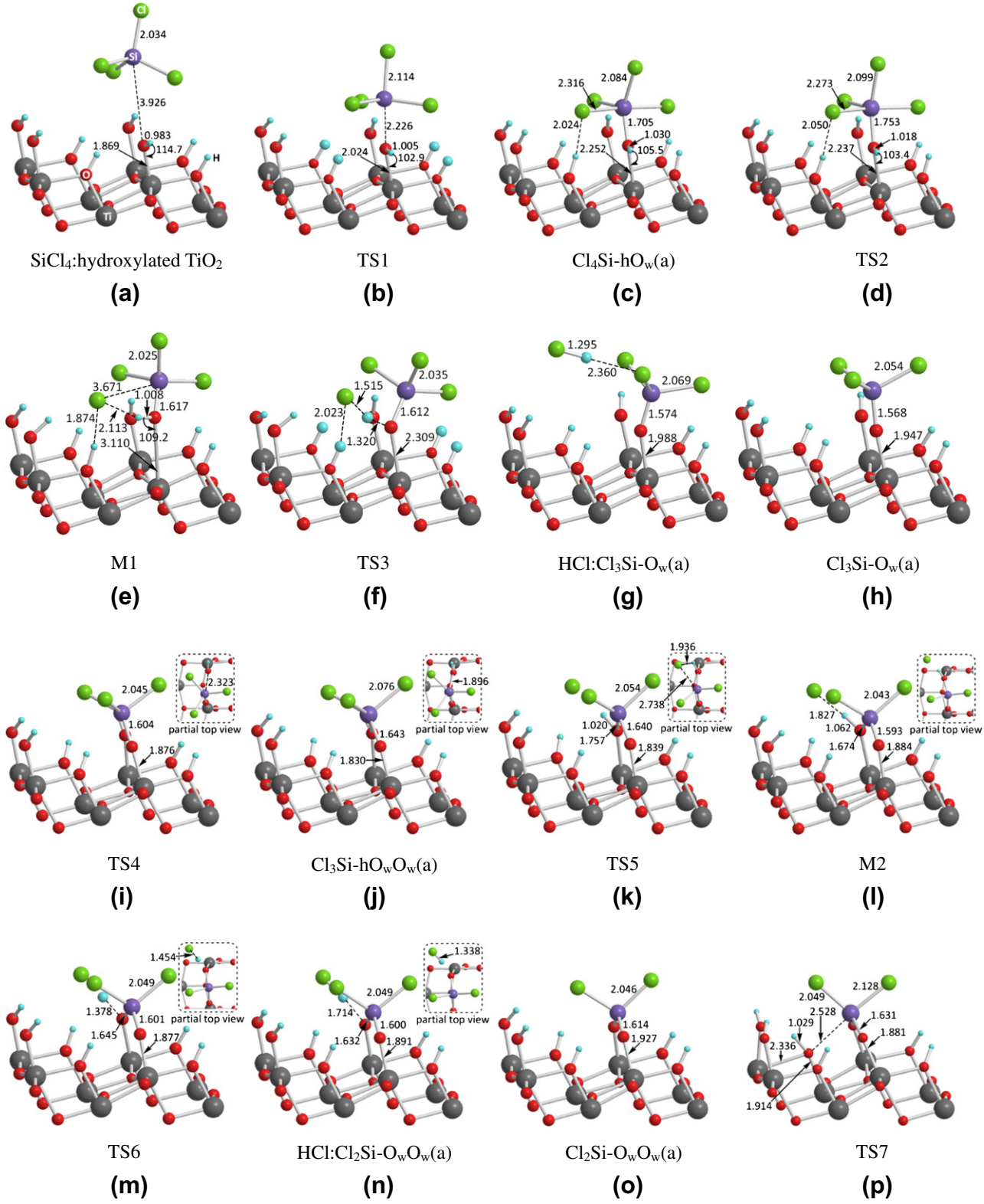

Fig. 4. Optimized geometries of adsorbed $SiCl_x$ on the hydroxylated TiO_2 anatase (1 0 1) surface. TiO_2 model is only shown with one Ti layer. The bond length and angle are in Å and degree, respectively.

energy barrier of 8.1 kcal/mol (**TS8**, Fig. 4r). The distance of the Cl...H hydrogen bonding in **M3** (Fig. 4s) is 2.085 Å. The third dehydrochlorination can occur by overcoming **TS9** (Fig. 4t) with a barrier of 10.3 kcal/mol and an exothermicity of 8.1 kcal/mol to form **HCl:ClSi–$O_sO_wO_w$(a)** (Fig. 4u). The HCl(g) can be released from **HCl:ClSi–$O_sO_wO_w$(a)** with only a small endothermicity of 0.3 kcal/mol. In **ClSi–$O_sO_wO_w$(a)**, all the H atoms are too far from the Cl atom to generate the fourth dehydrochlorination (Fig. 4v), it is left on the surface with an overall exothermicity of 7.0 kcal/mol from the reactants, $SiCl_4$(g) + hydroxylated anatase (1 0 1) TiO_2.

In the O_w-path described above, **Cl_3Si–O_w(a)** and **Cl_2Si–O_wO_w(a)** can be formed without thermal activation as all the transition

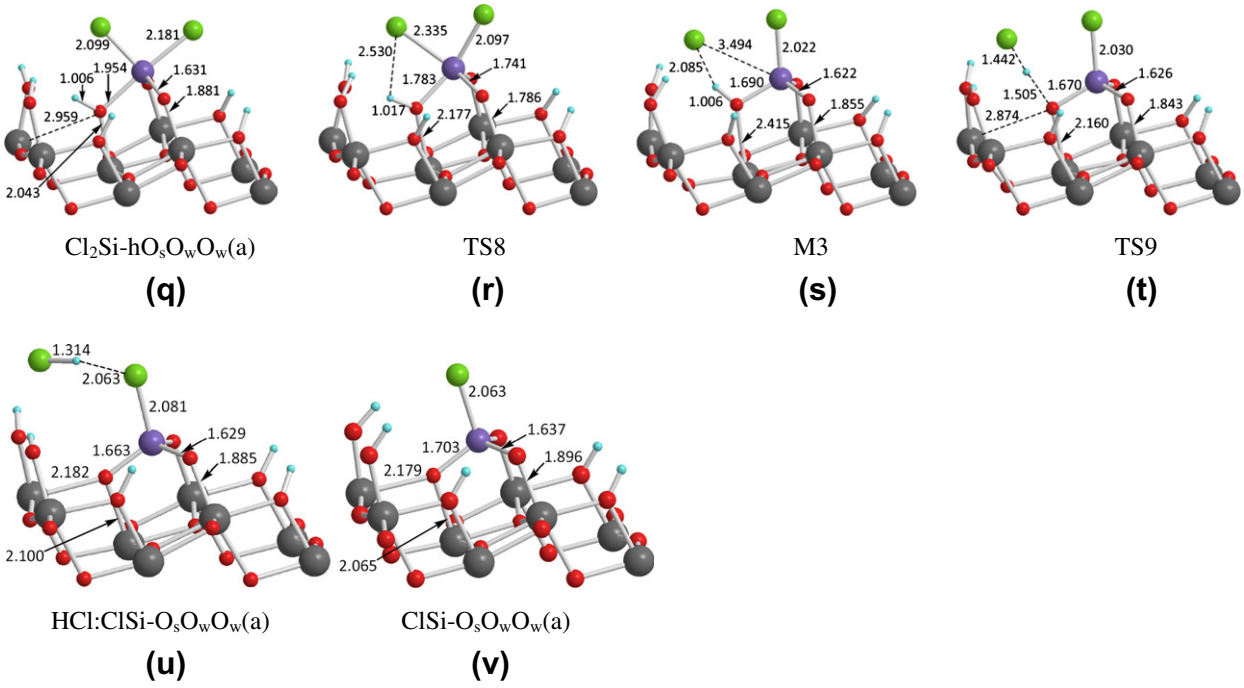

Fig. 4 (*continued*)

Table 1
Calculated adsorption energies of $SiCl_x$ on the hydroxylated TiO_2 surface (kcal/mol).

Adsorbate	Site	Figure	E_{ads}	Adsorbate	Site	Figure	E_{ads}
$SiCl_4$	hO_s	4a, S3a	11.5, 8.9	$SiCl_3$	O_s	S3q	112.5
	hO_w	4c	19.2		O_w	4h	133.2
$SiCl_3$	hO_sO_s	S3h	78.6	$SiCl_2$	O_sO_s	S3k	148.0
	hO_sO_w	S3ae	104.3		O_sO_w	S3ai	192.1
	hO_wO_s	S3s	105.7				
	hO_wO_w	4j	118.3		O_wO_w	4o	211.2
$SiCl_2$	$hO_sO_wO_w$	4q	185.1	SiCl	$O_sO_wO_w$	4v	313.0
	$hO_wO_sO_w$	S3ak	191.8				
	$hO_wO_sO_s$	S3m	186.3		$O_wO_sO_s$	S3ac	300.7
	$hO_sO_wO_s$	S3y	173.9				

states (**TS1–TS6**) are lower than the initial reactants. As a result, the most likely product in the energetically downhill reactions, **$Cl_2Si–O_wO_w$(a),** can be formed with an exothermicity of 27.0 kcal/mol relative to the reactants. The high barrier at **TS8** (33 kcal/mol) for its decomposition by dehydrogenation to **ClSi–$O_sO_wO_w$(a)** should make $Cl_2Si–O_wO_w$(a) the most abundant species produced in the reaction of $SiCl_4$ with the hydroxylated TiO_2 (101) anatase surface.

3.2.3. Adsorption energies

The adsorption energies of the species $SiCl_x$ on the hydroxylated TiO_2 surface are listed in Table 1. The adsorption energies were calculated by the following equation:

$$E_{ads} = -(E_{total} - E_{surf} - E_{gas})$$

where E_{total}, E_{gas}, and E_{surf} are the electronic energies of the adsorbed species on the surface, a gas-phase molecule, and the surface, respectively. The E_{surf} for **$Cl_3Si–hO_wO_w$(a),** for example, is the energy of a fully hydroxylated TiO_2 surface with one hydrogen vacancy for molecular adsorption.

As shown in Table 1, for the saturated **$Cl_{x-1}Si–P_1$...P_{4-x}(a)**, the average adsorption energies are 128, 170, and 307 kcal/mol for singly, doubly, and triply bonded configurations, respectively. The adsorption energies increase with the number of bondings. The same trend was noted for the over-bonded **$Cl_xSi–hP_1$...P_{4-x}(a)** with an Cl atom attached to the P_1 (oxygen) site, 13, 102, 184 kcal/mol, respectively. For the same number of binding sites, the adsorption energies of the over-bonded configurations are much lower than those of bond saturated configurations. As mentioned above, the gas phase molecules tend to adsorb on an 'O_w', which is supported by the adsorption energies shown in Table 1. In the case of SiH_x radical adsorptions (x = 1–3) [28], the adsorption energies of **$H_3Si–O_w$(a)** (133.2 kcal/mol), **$H_2Si–O_wO_w$(a)** (211.2 kcal/mol), **$HSi–O_sO_wO_w$(a)** (313.0 kcal/mol) are all larger than those of **$H_3Si–O_s$(a)** (97.6 and 112.5 kcal/mol), **$H_2Si–O_sO_s$(a)** (148.0 kcal/mol), **$HSi–O_wO_sO_s$(a)** (300.7 kcal/mol). A similar trend was observed in the over-bonded cases. Finally, these high adsorption energies also confirm the stability of $SiCl_x$ adsorption on the hydroxylated surface.

4. Conclusions

The $SiCl_x$ adsorption and reaction on the hydroxylated anatase (101) TiO_2 surface have been studied by periodic DFT calculations. The results firstly show that the hydroxylated anatase (101) TiO_2 surface can be formed spontaneously by the reaction $H_2O(g)$ +

anatase (101) TiO_2 surface. There are two kinds of oxygen adsorption sties, 'O_w' and 'O_s', on the fully hydroxylated surface. The adsorptions and reactions tend to occur more readily on the 'O_w' site than on the 'O_s' site based on the predicted adsorption energies. The stepwise decomposition of $SiCl_x$(a) can be achieved by dehydrochlorination, and the reaction paths can be divided into three types of pathways: O_w-path, O_s-path and cross-path. We find that the O_w-path is the most favored low energy path, followed by the cross-path and lastly the O_s-path. The adsorption and decomposition of $SiCl_4$ following the O_w-path can take place by three dehydrochlorination steps. Each dehydrochlorination can be achieved by three types of reactions: (1) $SiCl_x$ multi-site adsorptions; (2) the intermediate $\mathbf{M_x}$ (x = 1–3) formation; (3) the dehydrochlorination giving stable Cl_xSi(a) adsorbates (x = 1–3). We find that type (1) reactions control the $SiCl_x$ decomposition on the hydroxylated anatase (101) surface. **$Cl_3Si–O_w$(a)** and **$Cl_2Si–O_wO_w$(a)** can be formed without thermal activation; however, the formation of **$ClSi–O_sO_wO_w$(a)** needs to overcome a 33 kcal/mol energy barrier. Accordingly, the energetically downhill adsorption and decomposition reactions of $SiCl_4$ on the hydroxylated titania by stepwise dehydrochlorination processes is expected to produce **$Cl_2Si–O_wO_w$(a)** with the most abundant concentration providing a reactive and strong molecular linker for the growth of Si thin films and other semiconductor quantum dots for opto-electronic device and solar cell fabrication applications. Take the growth of a III–V metal nitride, for example, the Cl_2Si(O)O-functionalized surface can readily react with nitrogen and metal precursors (such as NH_3 and trimethyl indium) on the first surface layer as follows: $Cl_2Si(O)O(a) + NH_3 \rightarrow 2HCl + HNSi(O)O(a)$; $HNSi(O)O(a) + (CH_3)_3In \rightarrow (CH_3)_2InNSi(O)O(a) + CH_4$.

Acknowledgements

The authors are grateful to Taiwan's National Center for High-performance Computing for the CPU's facility and the National Science Council for the research support. MCL also wants to acknowledge Taiwan Semiconductor Manufacturing Co. for the TSMC Distinguished Professorship and Taiwan National Science Council for the Distinguished Visiting Professorship at the Center for Interdisciplinary Molecular Science, National Chiao Tung University, Hsinchu, Taiwan.

Appendix A. Supplementary material

Supplementary data associated with this article can be found, in the online version, at http://dx.doi.org/10.1016/j.comptc.2012.05.035.

References

[1] K.I. Hadjiivanov, D.G. Klissurski, Surface chemistry of titania (anatase) and titania-supported catalysts, Chem. Soc. Rev. 25 (1996) 61–69.
[2] A.L. Linsebigler, G. Lu, J.T. Yates, Photocatalysis on TiO_2 surfaces: principles, mechanisms, and selected results, Chem. Rev. 94 (1995) 735–758.
[3] M. Gratzel, Photoelectrochemical cells, Nature 414 (2001) 338–344.
[4] M.K. Nazeeruddin, A. Kay, I. Rodicio, R. Humphry-Baker, E. Muller, P. Liska, N. Vlachopoulos, M. Gratzel, Conversion of light to electricity by cis-X2bis(2,2′-bipyridyl-4,4′-dicarboxylate)ruthenium(II) charge-transfer sensitizers (X = Cl–, Br–, I–, CN–, and SCN–) on nanocrystalline titanium dioxide electrodes, J. Am. Chem. Soc. 115 (1993) 6382–6390.
[5] B. O'Regan, M. Gratzel, Solar energy conversion by dye-sensitized photovoltaic cells, Nature 353 (1991) 737–740.
[6] C.L. Huisman, A. Goossens, J. Schoonman, Aerosol synthesis of anatase titanium dioxide nanoparticles for hybrid solar cells, Chem. Mater. 15 (2003) 4617–4624.
[7] D. Li, C. Gu, C. Guo, C. Hu, The effects of ambient gases on the surface resistance of polyoxometalate/TiO_2 film, Chem. Phys. Lett. 385 (2004) 55–59.
[8] P. Yu, K. Zhu, A.G. Norman, S. Ferrere, A.J. Frank, A.J. Nozik, Nanocrystalline TiO_2 solar cells sensitized with InAs quantum dots, J. Phys. Chem. B 110 (2006) 25451–25454.
[9] J.L. Blackburn, D.C. Celmarten, A.J. Nozik, Electron transfer dynamics in quantum dot/titanium dioxide composites formed by in situ chemical bath deposition, J. Phys. Chem. B 107 (2003) 14154–14157.
[10] R. Vogel, P. Hoyer, H. Weller, Quantum-sized PbS, CdS, Ag_2S, Sb_2S_3, and Bi_2S_3 particles as sensitizers for various nanoporous wide-bandgap semiconductors, J. Phys. Chem. 98 (1994) 3183–3188.
[11] A. Shah, P. Torres, R. Tscharner, N. Wyrsch, H. Keppner, Photovoltaic technology: the case for thin-film solar cells, Science 285 (1999) 692–698.
[12] R.B. Bergmann, Crystalline Si thin-film solar cells: a review, Appl. Phys. A 69 (1999) 187–194.
[13] L. Stalmans, J. Poortmans, H. Bender, M. Caymax, K. Said, E. Vazsonyi, J. Nijs, R. Mertens, Porous silicon in crystalline silicon solar cells: a review and the effect on the internal quantum efficiency, Prog. Photovolt. Res. Appl. 6 (1998) 233–246.
[14] B. Hamilton, Porous silicon, Semicond. Sci. Technol. 10 (1995) 1187–1207.
[15] R.L. Smith, S.D. Collins, Porous silicon formation mechanisms, J. Appl. Phys. 71 (1992) R1–R22.
[16] A.G. Cullis, L.T. Canham, P.D.J. Calcott, The structural and luminescence properties of porous silicon, J. Appl. Phys. 82 (1997) 909–965.
[17] P.R. McCurdy, L.J. Sturgess, S. Kohli, E.R. Fisher, Investigation of the PECVD TiO_2–Si(100) interface, Appl. Surf. Sci. 233 (2004) 69–79.
[18] V.G. Erkov, S.F. Devyatova, E.L. Molodstova, T.V. Malsteva, U.A. Yanovskii, Si–TiO_2 interface evolution at prolonged annealing in low vacuum or N_2O ambient, Appl. Surf. Sci. 166 (2000) 51–56.
[19] P.G. Karlesson, J.H. Richter, M.P. Andersson, J. Blomquist, H. Siegbahn, P. Uvdal, A. Sandell, UHV-MOCVD growth of TiO_2 on SiO_x/Si(111): interfacial properties reflected in the Si 2p photoemission spectra, Surf. Sci. 580 (2005) 207–217.
[20] S. Takabayashi, R. Nakamura, Y. Nakato, A nano-modified Si/TiO_2 composite electrode for efficient solar water splitting, J. Photochem. Photobiol. A 166 (2004) 107–113.
[21] J. Abad, C. Rogero, J. Méndez, M.F. López, J.A. Martín-Gago, E. Román, Growth of subnanometer-thin Si overlayer on TiO_2 (110)-(1 × 2) surface, Appl. Surf. Sci. 234 (2004) 497–502.
[22] P. Raghunath, M.C. Lin, Adsorption configurations and reactions of boric acid on TiO_2 anatase (101) surface, J. Phys. Chem. C 112 (2008) 8276–8287.
[23] P. Raghunath, M.C. Lin, A computational study on the adsorption configurations and reactions of phosphorous acid on TiO_2 anatase (101) and rutile (110) surfaces, J. Phys. Chem. C 113 (2009) 3751.
[24] J.-G. Chang, J.-H. Wang, M.C. Lin, Adsorption configurations and energetics of BCl_x (x = 0–3) on TiO_2 anatase (101) and rutile (110) surfaces, J. Phys. Chem. A 111 (2007) 6746–6754.
[25] W.-F. Huang, H.-T. Chen, M.C. Lin, Density-functional theory study of the adsorption and reaction of H_2S on TiO_2 rutile (110) and anatase (101) surfaces, J. Phys. Chem. C 113 (2009) 20411–20420.
[26] W.-F. Huang, P. Raghunath, M.C. Lin, Computational study on the reactions of H_2O_2 on TiO_2 anatase (101) and rutile (110) surfaces, J. Comput. Chem. 32 (6) (2011) 1065–1081.
[27] C.-Y. Chang, H.-T. Chen, M.C. Lin, Adsorption configurations and reactions of nitric acid on TiO_2 rutile (110) and anatase (101) surfaces, J. Phys. Chem. C 113 (2009) 6140–6149.
[28] W.-F. Huang, H.-T. Chen, M.C. Lin, Density-functional calculations on the adsorption and reactions of SiH_x (x = 0–4) on TiO_2 anatase (101) and rutile (110) surfaces, Comput. Mater. Sci., submitted for publication.
[29] R.L. Kurtz, R. Stockbauer, T.E. Madey, E. Román, J.L.D. Segovia, Surf. Sci. 218 (1989) 178.
[30] M.B. Hugenschmidt, L. Gamble, C.T. Campbell, The interaction of H_2O with a TiO_2 (110) surface, Surf. Sci. 302 (1994) 329–340.
[31] P. Jones, J.A. Hockey, Infra-red studies of rutile surfaces. Part 1, Trans. Faraday Soc. 67 (1971) 2669–2678.
[32] P. Jones, J.A. Hockey, Infra-red studies of rutile surfaces. Part 2 – Hydroxylation, hydration and structure of rutile surfaces, Trans. Faraday Soc. 67 (1971) 2679–2685.
[33] L. Kavan, K. Kratochvilová, M. Gratzel, Study of nanocrystalline titanium dioxide (anatas) electrode in accumulation regime, J. Electroanal. Chem. 394 (1995) 93–102.
[34] Q.H. Powell, G.P. Fotou, T.T. Kodas, B.M. Anderson, Y. Guo, Gas-phase coating of TiO_2 with SiO_2 in a continuous flow hot-wall aerosol reactor, J. Mater. Res. 12 (1997) 552–559.
[35] C.-H. Hung, J.L. Katz, Formation of mixed oxide powders in flames: Part I. TiO.sub.2–SiO.sub.2, J. Mater. Res. 7 (1992) 1861–1869.
[36] P. Blochl, Projector augmented-wave method, Phys. Rev. B 17 (1994) 953–979.
[37] G. Kresse, J. Furthmuller, Efficiency of ab initio total energy calculations for metals and semiconductors using a plane-wave basis set, J. Comput. Mater. Sci. 6 (1996) 15.
[38] G. Kresse, J. Furthmuller, Efficient iterative schemes for ab initio total-energy calculations using a plane-wave basis set, Phys. Rev. B 54 (1996) 11169.
[39] J.P. Perdew, Y. Wang, Accurate and simple analytic representation of the electron-gas correlation energy, Phys. Rev. B 45 (1992) 13244–13249.
[40] J.-H. Wang, M.C. Lin, Reactions of hydrazoic acid and trimethyl indium on TiO_2 rutile (110) surface. A computational study on the formation of the first monolayer InN, J. Phys. Chem. B 110 (2006) 2263–2270.
[41] J.-H. Wang, M.C. Lin, Y.-C. Sun, Reactions of hydrazoic acid on TiO_2 nanoparticles: an experimental and computational study, J. Phys. Chem. B 109 (2005) 5133–5142.
[42] G. Mills, H. Jonsson, G.K. Schenter, Reversible work transition state theory: application to dissociative adsorption of hydrogen, Surf. Sci. 324 (1995) 305–337.

[43] K.D. Kim, S.H. Kim, H.T. Kim, Applying the Taguchi method to the optimization for the synthesis of TiO_2 nanoparticles by hydrolysis of TEOT in micelles, Colloids Surf. 254 (2005) 99–105.
[44] G.L. Li, G.H. Wang, Synthesis of nanometer-sized TiO_2 particles by a microemulsion method, Nanostruct. Mater. 11 (1999) 663–668.
[45] Y. Hwu, Y.D. Yao, N.F. Cheng, C.Y. Tung, H.M. Lin, X-ray absorption of nanocrystal TiO_2, Nanostruct. Mater. 9 (1997) 355–358.
[46] H. Zhang, J.F. Banfield, Thermodynamic analysis of phase stability of nanocrystalline titania, J. Mater. Chem. 8 (1998) 2073–2076.
[47] H. Zhang, J.F. Banfield, Understanding polymorphic phase transformation behavior during growth of nanocrystalline aggregates: insights from TiO_2, J. Phys. Chem. B 104 (2000) 3481–3487.
[48] M.R. Ranade, A. Navrotsky, H.Z. Zhang, J.F. Banfield, S.H. Elder, A. Zaban, P.H. Borse, S.K. Kulkarni, G.S. Doran, H.J. Whitfield, Energetics of nanocrystalline TiO_2, Proc. Natl. Acad. Sci. 99 (2002) 6476–6481.
[49] A.N. Enyashin, G. Seifert, Structure, stability and electronic properties of TiO_2 nanostructures, Phys. Status Solidi B 242 (2005) 1361–1370.
[50] N.G. Park, J.V.D. Lagemaat, A.J. Frank, Comparison of dye-sensitized rutile- and anatase-based TiO_2 solar cells, J. Phys. Chem. B 104 (2000) 8989–8994.
[51] S.D. Burnside, V. Shklover, C. Barbe, Pascal Comte, F. Arendse, K. Brooks, M. Greatzel, Self-organization of TiO_2 nanoparticles in thin films, Chem. Mater. 10 (1998) 2419–2425.
[52] B. O'Regan, M. Grätzel, A low-cost, high-efficiency solar cell based on dye-sensitized colloidal TiO_2 films, Nature 353 (1991) 737–740.
[53] F. Labat, P. Baranek, C. Adamo, Structural and electronic properties of selected rutile and anatase TiO_2 surfaces: an ab initio investigation, J. Chem. Theory Comput. 4 (2008) 341–352.
[54] J.K. Burdett, T. Hughbanks, G.J. Miller, J.W. Richardson Jr., J.V. Smith, Structural-electronic relationships in inorganic solids: powder neutron diffraction studies of the rutile and anatase polymorphs of titanium dioxide at 15 and 295 K, J. Am .Chem. Soc. 109 (1987) 3639–3646.
[55] C.J. Howard, T.M. Sabine, F. Dickson, Structural and thermal parameters for rutile and anatase, Acta Cryst. 47 (1991) 462–468.
[56] M. Horn, C.F. Schwerdtfeger, E.P. Meagher, Refinement of the structure of anatase at several temperatures, Z. Kristallogr 136 (1972) 273–281.
[57] A. Vittadini, A. Selloni, F.P. Rotzinger, M. Gratzel, Structure and energetics of water adsorbed at TiO_2 anatase (101) and (001) surfaces, Phys. Rev. Lett. 81 (1998) 2954–2957.
[58] M. Ramamoorthy, D. Vanderbilt, R.D. King-Smith, First-principles calculations of the energetics of stoichiometric TiO_2 surfaces, Phys. Rev. B 49 (1994) 16721–16727.
[59] A. Tilocca, A. Selloni, Vertical and lateral order in adsorbed water layers on anatase TiO_2(101), Langmuir 20 (2004) 8379–8384.
[60] G. Mattioli, F. Filippone, A.A. Bonapasta, Reaction intermediates in the photoreduction of oxygen molecules at the (101) TiO_2 (anatase) surface, J. Am. Chem. Soc. 128 (2006) 13772–13780.
[61] G.S. Herman, Z. Dohnalek, N. Ruzycki, U. Diebold, Experimental investigation of the interaction of water and methanol with anatase-TiO_2(101), J. Phys. Chem. B 107 (2003) 2788–2795.
[62] M.B. Hugenschmidt, L. Gamble, C.T. Campbell, The interaction of H_2O with a TiO_2(110) surface, Surf. Sci. 302 (1994) 329–340.
[63] G. Henkelman, A. Arnaldsson, H. Jonsson, A fast and robust algorithm for Bader decomposition of charge density, Comput. Mater. 36 (2006) 354–360.
[64] O. Sneh, M.L. Wise, A.W. Ott, L.A. Okada, S.M. George, Atomic layer growth of SiO_2 on Si(100) using $SiCl_4$ and H_2O in a binary reaction sequence, Surf. Sci. 334 (1995) 135–152.
[65] J.D. Ferguson, A.R. Yoder, A.W. Weimer, S.M. George, TiO_2 atomic layer deposition on ZrO_2 particles using alternating exposures of $TiCl_4$ and H_2O, Appl. Surf. Sci. 226 (2004) 393–404.